

## Article

# The Success of Fabrication of Pure SmFe<sub>2</sub> Phase Film with Outstanding Perpendicular Magnetic Anisotropy

Shijie Liao<sup>1,2,3</sup>, Fang Wang<sup>4</sup>, Hui Shen<sup>1,\*</sup>  and Jian Zhang<sup>2,3,\*</sup>

<sup>1</sup> School of Materials Science and Engineering, Shanghai Institute of Technology, Shanghai 201418, China; liaoshijie970907@163.com

<sup>2</sup> CAS Key Laboratory of Magnetic Materials and Devices, Ningbo Institute of Materials Technology and Engineering, Chinese Academy of Sciences, Ningbo 315201, China

<sup>3</sup> Zhejiang Province Key Laboratory of Magnetic Materials and Application Technology, Ningbo Institute of Materials Technology and Engineering, Chinese Academy of Sciences, Ningbo 315201, China

<sup>4</sup> School of Materials and Chemical Engineering, Ningbo University of Technology, Ningbo 315211, China; wangfangch@nbut.edu.cn

\* Correspondence: hshen@sit.edu.cn (H.S.); zhangj@nimte.ac.cn (J.Z.); Tel.: +86-13761712431 (H.S.); +86-574-86685341 (J.Z.)

**Abstract:** This study used DC magnetron sputtering technology to fabricate Sm-Fe films and systematically investigated the phase transition behavior of Sm-Fe films with different Fe ratios. It was found that at higher Fe content, the films consisted of Sm<sub>2</sub>Fe<sub>17</sub> or SmFe<sub>7</sub> phases; as Fe content decreased, the films were mainly composed of SmFe<sub>3</sub> or SmFe<sub>2</sub> phases; at higher Sm content, the films primarily consisted of Sm phase. Sm is prone to volatilization at high temperatures, so Ta was used as a capping layer to effectively suppress Sm volatilization, successfully synthesizing pure SmFe<sub>2</sub> phase films at a nearly 1:2 ratio. The magnetic properties and magnetostrictive behavior of the SmFe<sub>2</sub> films were investigated, revealing that pure-phase SmFe<sub>2</sub> films exhibit good perpendicular magnetic anisotropy and magnetostriction properties. The larger stress along the perpendicular-to-film direction, resulting from the absence of substrate-induced constraints, contributes to the excellent perpendicular magnetic anisotropy of the films. This study successfully synthesized pure-phase SmFe<sub>2</sub> films and discovered a new method for fabricating perpendicularly anisotropic films. The research findings are of great significance for the efficient synthesis of desired films with high phase formation temperatures containing volatile elements.

**Keywords:** magnetic films; perpendicular magnetic anisotropy; SmFe<sub>2</sub>



**Citation:** Liao, S.; Wang, F.; Shen, H.; Zhang, J. The Success of Fabrication of Pure SmFe<sub>2</sub> Phase Film with Outstanding Perpendicular Magnetic Anisotropy. *Materials* **2024**, *17*, 2027. <https://doi.org/10.3390/ma17092027>

Academic Editor: Antoni Planes

Received: 4 March 2024

Revised: 20 April 2024

Accepted: 22 April 2024

Published: 26 April 2024



**Copyright:** © 2024 by the authors. Licensee MDPI, Basel, Switzerland. This article is an open access article distributed under the terms and conditions of the Creative Commons Attribution (CC BY) license (<https://creativecommons.org/licenses/by/4.0/>).

## 1. Introduction

Magnetic anisotropy is a key characteristic of magnetic materials and plays an important role in various applications, such as spin electronic devices [1–4], microelectromechanical systems [5], magnetic nanosensors [6], magnetic storage [7], and magnetic recording [8,9]. In magnetic films, the easy magnetization direction is often preferentially oriented within the plane, making it difficult to obtain films with perpendicular magnetic anisotropy, which severely limits the development of high-performance functional devices [10,11]. Epitaxial growth is one effective method for fabricating films with perpendicular anisotropy [12]. However, the perpendicular anisotropy of epitaxial-grown films is influenced by various factors, such as growth conditions, crystal structure, lattice matching, and film thickness, among others [13,14].

Rare-earth transition metal intermetallic compound films exhibit excellent magnetic properties and have been widely used in magnetic microelectromechanical systems, among other fields [15,16]. Among the various rare-earth transition metal intermetallic compound films, Sm-based films such as Sm-Co and Sm-Fe have attracted considerable attention due to their excellent intrinsic magnetic properties. SmCo<sub>5</sub> and Sm<sub>2</sub>Co<sub>17</sub> in the Sm-Co

system are important magnetic phases.  $\text{SmCo}_5$  exhibits high coercivity and saturation magnetization, with coercivity reaching 15–35 kOe and a maximum energy product of 18–20 MGOe [17]. It also possesses a certain degree of temperature resistance [18]. However, its cost is higher due to the use of the rare element cobalt. On the other hand,  $\text{Sm}_2\text{Co}_{17}$  outperforms  $\text{SmCo}_5$  in terms of saturation magnetization, with a higher maximum energy product of 27 MGOe, but it is more expensive and temperature-sensitive [17].  $\text{Sm}_2\text{Co}_{17}$  and  $\text{SmCo}_5$  phases can be synthesized using physical or chemical methods to produce magnetically anisotropic permanent magnetic materials. Yue et al. successfully synthesized anisotropic  $\text{SmCo}_5$  nanochips with tailored morphologies by designing special-shaped hydroxide precursors. These nanochips exhibited a coercivity of 19.3 kOe and a maximum energy product of 14.4 MGOe [19]. Kumari et al. achieved high magnetic anisotropy in composite materials by chemically synthesizing a combination of soft magnetic Co phase and hard magnetic Sm-Co phase [20]. Sm-Fe films exist in multiple phases, including the amorphous phase,  $\text{SmFe}_2$ ,  $\text{SmFe}_3$ , and  $\text{Sm}_2\text{Fe}_{17}$ , etc. Compared to the  $\text{SmFe}_2$  phase, both the  $\text{SmFe}_3$  and  $\text{Sm}_2\text{Fe}_{17}$  phases demonstrate higher saturation magnetization and coercivity ( $\text{SmFe}_3$ :  $M_s = 80$  emu/g,  $H_c = 3100$  Oe;  $\text{Sm}_2\text{Fe}_{17}$ :  $M_s = 100$  emu/g,  $H_c = 680$  Oe) [21–24]. In contrast, the reported saturation magnetization and coercivity of the  $\text{SmFe}_2$  phase are 59.8 emu/g and 300 Oe, respectively [25,26]. Notably, among these phases,  $\text{SmFe}_2$  demonstrates exceptional magnetostrictive properties. Due to the presence of multiple phases in Sm-Fe films, it is challenging to obtain pure phase  $\text{SmFe}_2$ . Wang et al. discovered that thermal sputtering and heat treatment processes can lead to the formation of  $\text{SmFe}_2$  phase, but they also observed the presence of  $\alpha$ -Fe, Sm, oxides, and other impurity phases [27]. Yoon et al. found that Sm-Fe films can be transformed into  $\text{SmFe}_2$  through high-temperature annealing, but Fe precipitation occurs as well [28]. However, current research on Sm-Fe films mostly focuses on the synthesis of simple amorphous films. For instance, Honda et al. fabricated cantilever actuators and movable devices composed of amorphous Tb-Fe and Sm-Fe films, demonstrating characteristics such as large deflection and wireless driving. The magnetostriction coefficient of SmFe films under a 1000 Oe magnetic field ranges from  $-250$  ppm to  $-300$  ppm, and they exhibit in-plane magnetic anisotropy [29,30]. Quandt and Seemann prepared amorphous Tb-Dy-Fe and Sm-Fe films and designed and manufactured actuators for finite element analysis, demonstrating great potential for application in microsystems. The SmFe films exhibit an in-plane magnetic easy axis, and the magnetostriction coefficient reaches a maximum of around  $-350$  ppm under a bias voltage of 120 V and a 6000 Oe magnetic field [31]. Currently, the coercivity of the SmFe amorphous phase can reach 265 Oe [32]. Therefore, the challenge lies in preparing  $\text{SmFe}_2$  films with high magnetic performance, and successfully synthesizing  $\text{SmFe}_2$  films with perpendicular magnetic anisotropy is also an intriguing research topic.

In this work, we successfully prepared  $\text{SmFe}_2$  films with perpendicular magnetic anisotropy and high magnetic performance using DC magnetron sputtering. We systematically investigated the phase formation behavior of SmFe films with different Fe composition ratios. We found that at higher Fe content, the films consist of  $\text{Sm}_2\text{Fe}_{17}$  or  $\text{SmFe}_7$  phases, while a decrease in Fe content enables the formation of the  $\text{SmFe}_2$  phase. In the absence of a capping layer, Sm has high volatility at elevated temperatures, resulting in the formation of  $\text{SmFe}_7$  or  $\text{SmFe}_3$  phases under compositions close to those of  $\text{SmFe}_2$ . To ensure the formation of the  $\text{SmFe}_2$  phase, the high-temperature evaporation of Sm can be compensated by appropriately increasing the Sm content in the stoichiometric ratio. Moreover, since Ta exhibits good ductility and resistance to oxidation, it is chosen to be deposited as a covering layer on SmFe films. By depositing a Ta capping layer, the volatilization of Sm is effectively suppressed, ensuring the high-temperature phase formation of near-stoichiometric  $\text{SmFe}_2$  polycrystalline films. Finally, we investigate the magnetic and magnetostrictive properties of the  $\text{SmFe}_2$  polycrystalline films. It is found that the films exhibit small stress in the parallel film plane direction due to substrate constraint but large stress in the perpendicular film plane direction, resulting in good perpendicular magnetic anisotropy.

## 2. Materials and Methods

The Sm-Fe film is prepared using the DC magnetron sputtering technique, with a sputtering chamber vacuum of  $2\text{--}3 \times 10^{-6}$  Pa. Both Fe (99.99%) and Sm (99.99%) targets are used for sputtering; the Sm-Fe film is deposited using the co-sputtering method. The film thickness is measured using a scanning probe microscope (SPM, Dimension-ICON, Bruker, Marlborough City, MA, USA) according to the thickness of the deposited film after a certain period of time, and the deposition rate of the film is calculated. The elemental composition of the Sm-Fe film is adjusted based on the sputtering power of the Sm and Fe targets. The Sm-Fe film, with a thickness of approximately 1  $\mu\text{m}$ , is deposited on a 500  $\mu\text{m}$  thick (100) Si substrate, with a tantalum (Ta) layer serving as both a buffer and a cover layer. Two types of films are prepared:  $\text{SmFe}_x(\text{T})/\text{Ta}(\text{AA})$  ( $x = 0.25\text{--}1.6/1.9$ ,  $T = 500\text{ }^\circ\text{C}/700\text{ }^\circ\text{C}$ ) and  $\text{SmFe}_x(\text{T})/\text{Ta}(\text{BA})$  ( $x = 1.5\text{--}9$ ,  $T = 250\text{ }^\circ\text{C}\text{--}700\text{ }^\circ\text{C}$ ), where  $x$  represents the Fe composition,  $T$  indicates the deposition temperature, AA indicates the deposition of a Ta cover layer after annealing, and BA indicates the deposition of a Ta cover layer before annealing. The annealing time is 15 min to 1 h. Argon gas (5N) is used as the sputtering gas at a pressure of 0.8 Pa.

The phases of the Sm-Fe film are analyzed using an X-ray diffraction analyzer (XRD, D8 ADVANCE, Bruker, Bremen, Germany). The magnetic properties of the Sm-Fe film are measured using a vibrating sample magnetometer (VSM, Lakeshore 7410, Lakeshore, Carson, CA, USA). The surface and cross-sectional morphology of the Sm-Fe film are characterized using scanning electron microscopy (SEM, G300, ZEISS, Jena, Germany) with energy-dispersive X-ray spectroscopy (EDS), and the cross-sectional morphology is observed using hand-broken samples. The magnetostrictive coefficient of the Sm-Fe film is measured by a material magnetostrictive characteristic measuring instrument (BKT-2600, BEIJING SHINCO TEST SCIENCE AND TECHNOLOGY CO. LTD, Beijing, China), with a maximum parallel magnetic field of  $\Delta H_{\parallel} = 1\text{ T}$ .

## 3. Results and Discussion

### 3.1. XRD Analysis

The investigated study focuses on high-temperature deposition, followed by subsequent annealing, and the phase formation behavior of Sm-Fe films with varying Fe composition ratios  $x$  by depositing a Ta protective layer on top after high-temperature annealing. Table 1 presents the crystallographic basic information of potential phases existing in Sm-Fe films. The peaks at  $2\theta = 33^\circ$ ,  $61^\circ$  and  $70^\circ$  are from the Si substrate [33]. Figure 1a shows the XRD patterns of  $\text{SmFe}_x(500\text{ }^\circ\text{C})/\text{Ta}(\text{AA})$  films annealed at  $700\text{ }^\circ\text{C}$  for composition ratios  $x = 0.25\text{--}1.9$ . It can be observed that the  $\text{SmFe}_3$  phase forms at composition  $x = 1.9$ , while the  $\text{SmFe}_2$  phase, along with a small amount of Sm phase, can be formed for the film of  $x = 1$ , indicating the effectiveness of the Ta coating layer due to the absence of Sm oxide phase. Moreover, decreasing the Fe composition ratio to  $x = 0.5$  or  $0.25$  results in the disappearance of the  $\text{SmFe}_2$  phase, with the Sm-Fe film primarily composed of the Sm phase. Figure 1b presents the XRD patterns of  $\text{SmFe}_x(700\text{ }^\circ\text{C})/\text{Ta}(\text{AA})$  films deposited at high temperatures without subsequent annealing treatments for  $x = 0.25\text{--}1.6$ . For the composition  $x = 1.6$ , the film is mainly composed of the low-Sm-content  $\text{SmFe}_7$  phase. Further reducing the Fe content to a composition ratio of 1:1 in Sm-Fe films leads to the appearance of the  $\text{SmFe}_2$  phase, along with the presence of  $\text{SmFe}_3$  and Sm phases. When the Fe content decreases to a composition ratio of  $x = 0.5$ , the dominant phase is  $\text{SmFe}_2$ , with a small amount of Sm phase also present. Finally, at the lowest Fe composition ratio of  $x = 0.25$ , the  $\text{SmFe}_2$  phase disappears, and the film is mainly composed of the Sm phase. From the above experiments, it can be found that the composition ratio required for the formation of the  $\text{SmFe}_2$  main phase is significantly higher than the stoichiometric ratio of  $\text{SmFe}_2$ , indicating the high volatility of Sm during the thermal deposition and annealing processes. Additionally,  $700\text{ }^\circ\text{C}$  deposition of the film samples with a composition ratio of  $\text{SmFe}_{0.5}$  leads to the formation of the  $\text{SmFe}_2$  main phase, while films with the Sm-Fe composition ratio deposited at  $500\text{ }^\circ\text{C}$  and subsequently annealed at  $700\text{ }^\circ\text{C}$  exhibit the formation of the

SmFe<sub>2</sub> main phase. This suggests that Sm has a higher volatility during high-temperature deposition, requiring a higher Sm composition ratio for the formation of the SmFe<sub>2</sub> phase.

**Table 1.** The table shows the space group, crystal structure type, and lattice parameters of different phases according to the JCPDS (Joint Committee on Powder Diffraction Standards) card numbers.

Phase	Space Group	Structure Type	Lattice Constant (Å)
SmFe <sub>7</sub> (JCPDS#19-0621)	R-3m	TbCu7	a = 8.554 c = 12.441
Sm <sub>2</sub> Fe <sub>17</sub> (JCPDS#49-1412)	R-3m	Th2Zn17	a = 8.563 c = 12.455
SmFe <sub>3</sub> (JCPDS#50-1450)	R-3m	PuNi3	a = 5.179 c = 24.795
SmFe <sub>2</sub> (JCPDS#25-1152)	Fd3m	MgCu2	a = 7.415 c = 3.629
Sm (JCPDS#06-0419)	R-3m	—	a = 3.629 c = 26.203
Ta (JCPDS#04-0788)	Im3m	—	a = 3.305

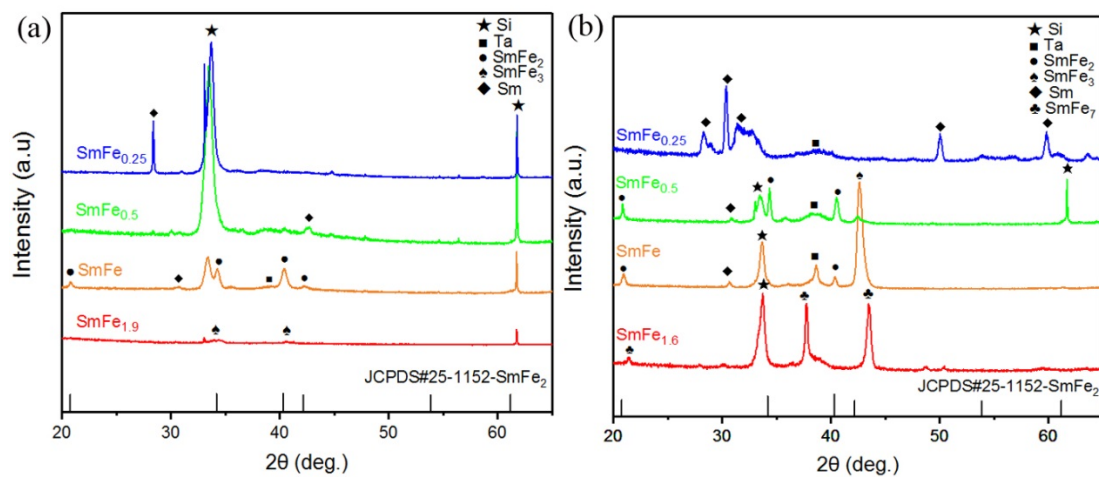


**Figure 1.** (a) XRD patterns of SmFe<sub>x</sub> ( $x = 0.25$ – $1.9$ ) films deposited at  $500\text{ }^{\circ}\text{C}$  and annealed at  $700\text{ }^{\circ}\text{C}$  for 1 h (with Ta capping layer after annealing); (b) XRD patterns of SmFe<sub>x</sub> ( $x = 0.25$ – $1.6$ ) films deposited at  $700\text{ }^{\circ}\text{C}$  (with Ta capping layer after high-temperature deposition).

In order to mitigate the negative effects of volatile Sm during high-temperature annealing on the formation of the SmFe<sub>2</sub> phase, a Ta capping layer was applied to the Sm-Fe film before high-temperature annealing to prevent Sm volatilization. The phase transition behavior of this kind of Sm-Fe films with different composition ratios, deposition temperatures, and annealing times was investigated. Figure 2a presents the XRD diffraction patterns of the SmFe<sub>x</sub>( $300\text{ }^{\circ}\text{C}$ )/Ta(BA) film with a composition of  $x$  ranging from 1.5 to 9, annealed at  $700\text{ }^{\circ}\text{C}$  for 0.5 h. It can be observed that when the composition is  $x = 9$ , the film is mainly composed of Sm<sub>2</sub>Fe<sub>17</sub> with an additional strong  $\alpha$ -Fe diffraction peak. Further reducing the Fe composition to  $x = 4$  results in the disappearance of the  $\alpha$ -Fe phase [33]. For  $x = 3$  and 4, the film is mainly composed of Sm<sub>2</sub>Fe<sub>17</sub> and SmFe<sub>3</sub> phases. At  $x = 2$ , the Sm<sub>2</sub>Fe<sub>17</sub> phase vanishes, and the Sm-Fe film is mainly composed of SmFe<sub>2</sub> and SmFe<sub>3</sub> phases. At  $x = 1.9$ , the film can form the SmFe<sub>2</sub> phase, but a small amount of the SmFe<sub>3</sub> phase is also present. When  $x$  is further reduced to 1.5 and 1.6, Sm diffraction peaks appear, indicating an excessive addition of Sm. The experimental results reveal that the composition range for the formation of the main SmFe<sub>2</sub> phase in the film, with the Ta capping layer applied before annealing, is  $x = 1.8$ – $2$ . Within this composition range, the Sm content in the film is much lower compared to the film with the Ta capping layer applied after annealing, affirming the effectiveness of the Ta capping layer in suppressing Sm volatilization.

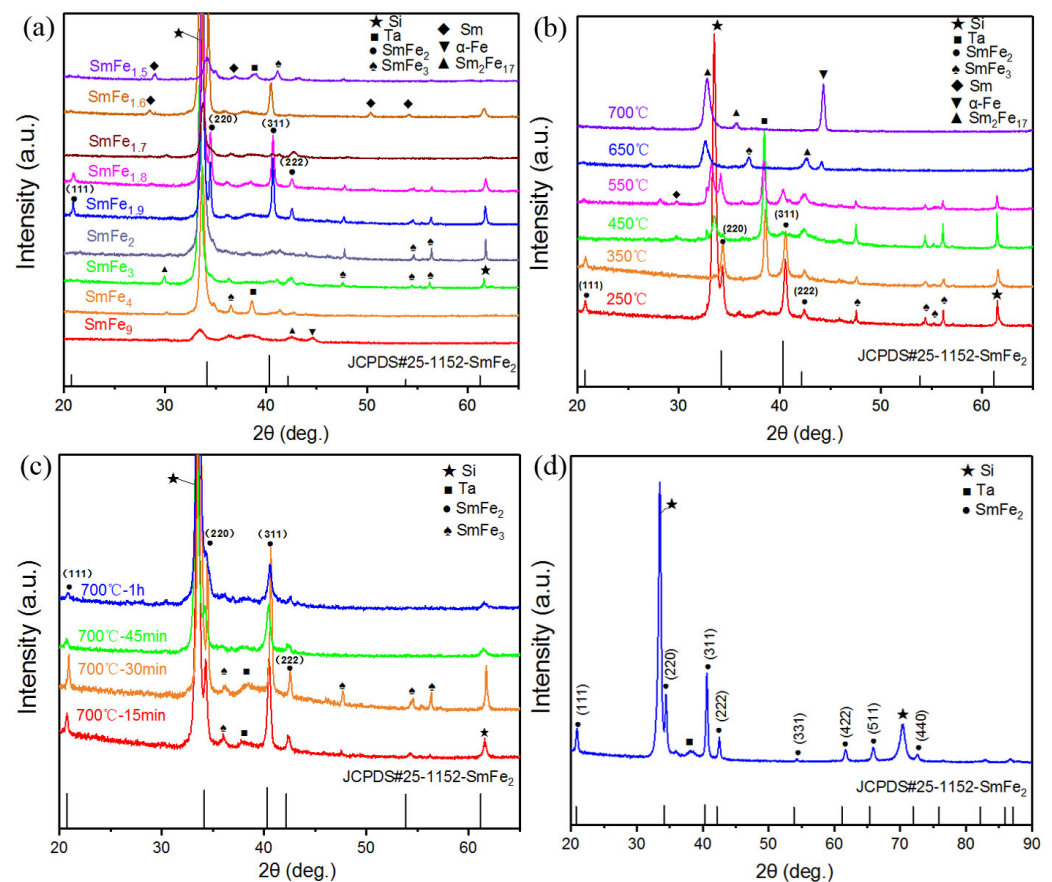


**Figure 2.** (a) XRD patterns of films deposited with  $\text{SmFe}_x$  ( $x = 1.5\text{--}9$ ) layer at  $300\text{ }^\circ\text{C}$ , followed by deposition of a  $50\text{ nm}$  Ta capping layer and then annealing at  $700\text{ }^\circ\text{C}$  for  $0.5\text{ h}$ . (b) XRD patterns of films deposited with  $\text{SmFe}_2$  layer at different temperatures ( $250\text{ }^\circ\text{C}$  to  $700\text{ }^\circ\text{C}$ ), followed by deposition of a  $50\text{ nm}$  Ta capping layer and then annealing at  $700\text{ }^\circ\text{C}$  for  $0.5\text{ h}$ . (c) XRD patterns of films deposited with  $\text{SmFe}_2$  layer at  $300\text{ }^\circ\text{C}$ , followed by deposition of a  $50\text{ nm}$  Ta capping layer and annealing at different times ( $15\text{ min}$  to  $1\text{ h}$ ) at  $700\text{ }^\circ\text{C}$ . (d) XRD patterns of films were deposited with  $\text{SmFe}_{1.9}$  layer at  $500\text{ }^\circ\text{C}$ , followed by deposition of a  $50\text{ nm}$  Ta capping layer and then annealing at  $700\text{ }^\circ\text{C}$  for  $1\text{ h}$ .

Based on the determination of the composition range for the formation of the main  $\text{SmFe}_2$  phase from Figure 2a, Sm-Fe films with different deposition temperatures were prepared to find the optimal deposition temperature. These films were then subjected to high-temperature annealing with a Ta capping layer applied before annealing. Figure 2b shows the XRD patterns of  $\text{SmFe}_2(250\text{ }^\circ\text{C}\text{--}700\text{ }^\circ\text{C})/\text{Ta}(\text{BA})$  films deposited at various temperatures. Within the temperature range of  $250\text{ }^\circ\text{C}\text{--}550\text{ }^\circ\text{C}$ , the films can form the main  $\text{SmFe}_2$  phase with a small amount of  $\text{SmFe}_3$  phase. Notably, the films deposited at  $250\text{ }^\circ\text{C}$  and  $350\text{ }^\circ\text{C}$  exhibit a lower proportion of  $\text{SmFe}_3$  phase compared to those deposited at  $450\text{ }^\circ\text{C}$  and  $550\text{ }^\circ\text{C}$ . When the deposition temperature is increased to  $650\text{ }^\circ\text{C}$ , the  $\alpha\text{-Fe}$  phase, which had disappeared for  $x = 4$ , reappears. Moreover, when the deposition temperature is raised to  $700\text{ }^\circ\text{C}$ , the intensity of the  $\alpha\text{-Fe}$  diffraction peak increases [27], indicating an elevated Sm volatilization rate. Therefore, only at lower deposition temperatures can the high-Sm-containing  $\text{SmFe}_2$  and  $\text{SmFe}_3$  phases form.

Figure 2c displays the XRD patterns of the  $\text{SmFe}_2(300\text{ }^\circ\text{C})/\text{Ta}(\text{BA})$  film with a composition of  $x = 2$ , annealed at  $700\text{ }^\circ\text{C}$  for different durations. For annealing times of  $15\text{ min}\text{--}30\text{ min}$ , the film is mainly composed of  $\text{SmFe}_2$  and  $\text{SmFe}_3$  phases. As the annealing time reaches  $45\text{ min}$ , a pure phase of polycrystalline  $\text{SmFe}_2$  film is formed. Compared to the  $45\text{-minute}$  annealed sample, the film annealed for  $1\text{ h}$  should exhibit a larger grain size in the  $\text{SmFe}_2$  phase.

Based on the experimental results shown in Figure 2a–c, the conditions for the formation of the  $\text{SmFe}_2$  phase in the film are determined to be a composition ratio within  $x = 1.8\text{--}2$ , a deposition temperature within  $250\text{--}550\text{ }^\circ\text{C}$ , and an annealing time within  $45\text{ min--}1\text{ h}$ . As a further example, a  $\text{SmFe}_{1.9}$  film with a composition ratio of  $x = 1.9$  was prepared and annealed at  $700\text{ }^\circ\text{C}$  for 1 h, as shown in Figure 2d. It can be observed that a pure phase of polycrystalline  $\text{SmFe}_2$  film is formed in this sample. Our research results from Figures 1 and 2 demonstrate that the deposition of a Ta capping layer effectively prevents Sm volatilization. By adjusting the deposition temperature and annealing time close to the proper composition ratio for the  $\text{SmFe}_2$  phase, we have successfully fabricated a single-phase polycrystalline  $\text{SmFe}_2$  film.

### 3.2. Magnetic Performance Analysis

We have investigated the magnetic properties of the prepared Sm-Fe film samples. Figure 3a shows the magnetic hysteresis loop of the  $\text{SmFe}_{1.9}(500\text{ }^\circ\text{C})/\text{Ta}(\text{BA})$  film samples of as-deposited and annealed at  $700\text{ }^\circ\text{C}$  for 1 h, respectively, along the direction perpendicular to the film surface. Compared with annealed samples, the as-deposited sample exhibits a low coercivity of 641 Oe and a saturation magnetization of 30.9 emu/g, possibly due to the poor crystallinity of the as-deposited film. After annealing at  $700\text{ }^\circ\text{C}$ , the  $\text{SmFe}_{1.9}(500\text{ }^\circ\text{C})/\text{Ta}(\text{BA})$  film transforms into a polycrystalline  $\text{SmFe}_2$  film, resulting in higher coercivity and saturation magnetization. The coercivity reaches 2427 Oe, while the saturation magnetization and residual magnetization are 68.6 emu/g and 48.4 emu/g, respectively. These values are significantly higher than those previously reported, and compositions with ratios close to  $\text{SmFe}_2$  films can achieve a maximum coercivity of 650 Oe [32–36]. Samata et al. reported a saturated magnetization of 59.8 emu/g for polycrystalline grown using the self-flux method, while the saturated magnetization of the films we prepared was 68.6 emu/g, slightly higher than their reported value [25]. Figure 3b shows the magnetic hysteresis loops of the  $\text{SmFe}_{1.9}(500\text{ }^\circ\text{C})/\text{Ta}(\text{BA})\text{--}(700\text{ }^\circ\text{C}, 1\text{ h})$ ,  $\text{SmFe}(500\text{ }^\circ\text{C})/\text{Ta}(\text{AA})\text{--}(700\text{ }^\circ\text{C}, 1\text{ h})$ , and  $\text{SmFe}_{0.5}(500\text{ }^\circ\text{C})/\text{Ta}(\text{AA})$  film samples along the parallel and perpendicular directions to the film surface. The saturation magnetization along the perpendicular direction is higher than that along the parallel direction for all these samples. This is because the different preparation conditions lead to the formation of the  $\text{SmFe}_2$  main phase in all the Sm-Fe films, and the excellent magnetostrictive properties of the  $\text{SmFe}_2$  phase induce stress in the films under high magnetic fields. The presence of the Si substrate restricts the stress magnitude along the parallel direction, resulting in lower coercivity and saturation magnetization. On the other hand, there is no restriction on stress along the perpendicular direction, resulting in higher values for coercivity and saturation magnetization. According to the Scherrer formula:  $D = k\lambda/\beta\cos\theta$ , where  $k$  is the Scherrer constant (typically 0.89),  $\lambda$  is the X-ray wavelength,  $\theta$  is the Bragg diffraction angle, and  $\beta$  is the full width at half maximum of the diffraction peak. The crystallite size  $\text{SmFe}_{1.9}(500\text{ }^\circ\text{C})/\text{Ta}(\text{BA})\text{--}(700\text{ }^\circ\text{C}, 1\text{ h})$ ,  $\text{SmFe}(500\text{ }^\circ\text{C})/\text{Ta}(\text{AA})\text{--}(700\text{ }^\circ\text{C}, 1\text{ h})$ , and  $\text{SmFe}_{0.5}(500\text{ }^\circ\text{C})/\text{Ta}(\text{AA})$  samples were calculated to be 31.1 nm, 21 nm, and 30 nm, respectively. The significant difference in magnetic properties may be due to the formation of pure  $\text{SmFe}_2$  phase in  $\text{SmFe}_{1.9}(500\text{ }^\circ\text{C})/\text{Ta}(\text{BA})\text{--}(700\text{ }^\circ\text{C}, 1\text{ h})$  sample, without the non-magnetic Sm phase. In addition, applying a magnetic field along the perpendicular direction generates higher stress, leading to superior magnetic properties compared to other Sm-Fe films. Our results indicate a novel strategy to develop perpendicular anisotropy in films. Figure 3c shows the magnetostrictive coefficient ( $\lambda$ ) of the 1:2 phase films prepared at different deposition temperatures and annealing times for  $\text{SmFe}_{1.9}(\text{T})/\text{Ta}(\text{BA})$  films. At the same deposition temperature, a longer annealing time results in a larger magnetostrictive coefficient ( $\lambda$ ) for the Sm-Fe films. This is possibly due to the larger grain size obtained with longer annealing times, indicating that prolonged annealing enhances the magnetostrictive coefficient of the films. Additionally, the magnetostrictive coefficient of the sample deposited at  $550\text{ }^\circ\text{C}$  and annealed at  $700\text{ }^\circ\text{C}$  for 30 min is higher than that of the sample deposited at  $300\text{ }^\circ\text{C}$  and annealed at  $700\text{ }^\circ\text{C}$  for 45 min, suggesting that higher temperature deposition and annealing lead to higher

purity of the  $\text{SmFe}_2$  phase. However, the maximum magnetostrictive coefficient achieved in the Sm-Fe films we prepared is  $-234$  ppm, which is lower than the values reported in the literature [37,38]. This may be attributed to the high thickness of the Si substrate used for depositing the Sm-Fe films, which affects the magnitude of stress [39].

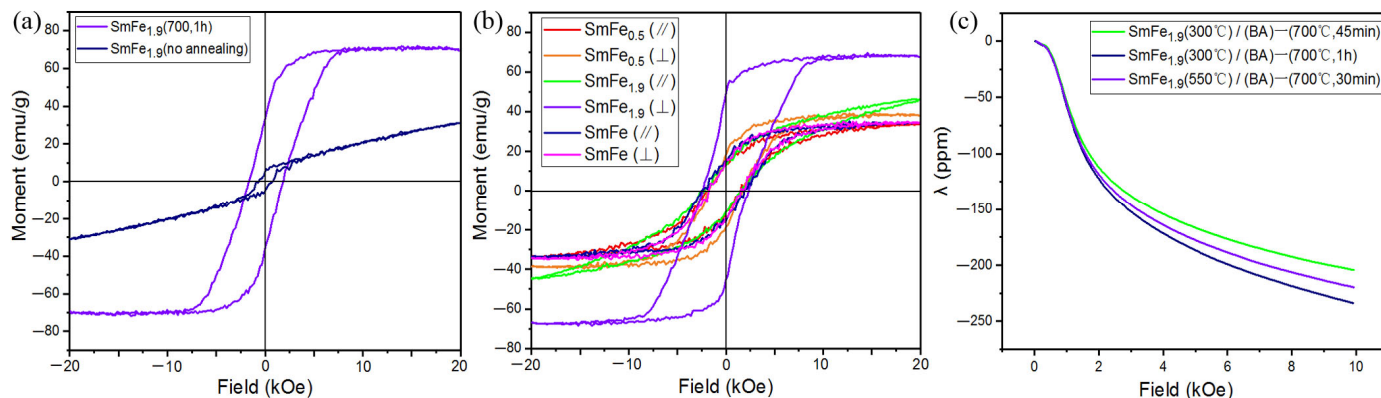


**Figure 3.** (a) Magnetic hysteresis loop of the  $\text{SmFe}_{1.9}(500^\circ\text{C})/\text{Ta}(\text{BA})$  film samples in the perpendicular film plane direction, both as-deposited and annealed at  $700^\circ\text{C}$  for 1 h ( $\text{SmFe}_{1.9}(500^\circ\text{C})/\text{Ta}(\text{BA})-(700^\circ\text{C}, 1\text{ h})$ ); (b) Magnetic hysteresis loops of the  $\text{SmFe}_{1.9}(500^\circ\text{C})/\text{Ta}(\text{BA})$  film annealed at  $700^\circ\text{C}$  for 1 h, as well as the  $\text{SmFe}(500^\circ\text{C})/\text{Ta}(\text{AA})$  film annealed at  $700^\circ\text{C}$  for 1 h and the as-deposited  $\text{SmFe}_{0.5}(500^\circ\text{C})/\text{Ta}(\text{AA})$  film sample in parallel (//) and perpendicular ( $\perp$ ) directions; (c) Magnetostrictive coefficient chart of the  $\text{SmFe}_{1.9}(500^\circ\text{C})/\text{Ta}(\text{BA})$  film annealed at different times at  $700^\circ\text{C}$ .

### 3.3. Morphology Analysis

Figure 4 illustrates the surface and cross-sectional morphology of the film sample  $\text{SmFe}_{1.9}(500^\circ\text{C})/\text{Ta}(\text{BA})-(700^\circ\text{C}, 1\text{ h})$ , and the elemental distribution on the surface of the film sample was analyzed using EDS. Examining the cross-section of the film provides information about its density and thickness. Figure 4a presents the SEM image of the cross-section of the film sample, revealing a thickness of approximately  $1\ \mu\text{m}$  for the Sm-Fe film, which closely matches the design based on deposition rate. The film contains a small amount of pores of different sizes. Figure 4b shows the SEM image of the film surface, which appears remarkably smooth. The locally enlarged SEM image of the  $\text{SmFe}_2(550^\circ\text{C})/\text{Ta}(\text{BA})$  sample annealed at  $700^\circ\text{C}$  for 0.5 h is placed in the upper right corner of Figure 4b. According to the image, the estimated grain size is  $135.6\ \text{nm}$ , which is larger than the grain size calculated by the Scherrer formula. The possible reason for this is that the deposited Ta coating layer has enlarged the grains. Figure 4c,d display the distribution of Sm and Fe elements on the film surface, demonstrating a relatively uniform distribution throughout the entire surface of the sample. Through quantitative analysis of the Sm and Fe content, it was found that the content of Sm and Fe is 29 at% and 71 at%, respectively, which closely aligns with the compositional ratio of Sm and Fe. This further proves that the deposition of the Ta covering layer effectively prevents the volatilization of Sm during high-temperature heat treatment of the Sm-Fe film.

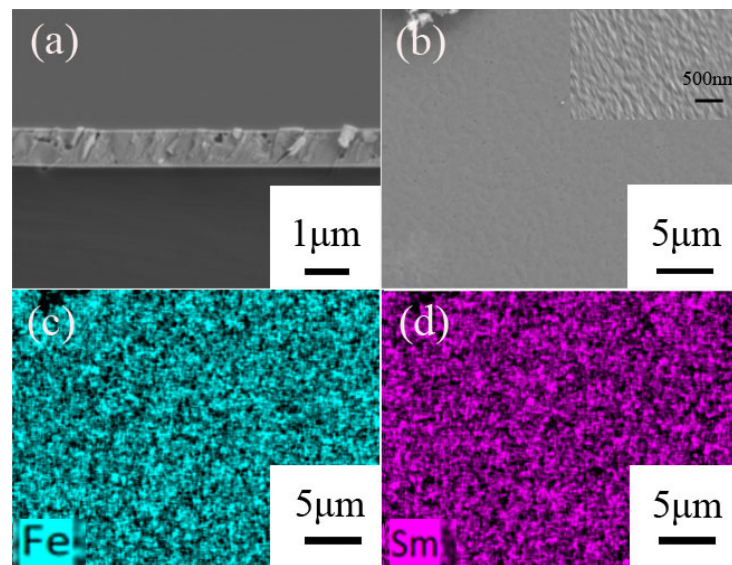


**Figure 4.** SEM and EDS images of the annealed (700 °C, 1 h) SmFe<sub>1.9</sub>(500 °C)/Ta(BA) film: (a) Cross-sectional SEM image of the film; (b) Surface SEM image of the film; (c) Elemental distribution of Fe in the film surface; (d) Elemental distribution of Sm in the film surface.

#### 4. Conclusions

This work employs an ultra-high vacuum magnetron sputtering system to fabricate Sm-Fe films and systematically investigate the influence of different Fe content, deposition temperature, and annealing time on the phase formation in Sm-Fe films. Without depositing a Ta layer and performing high-temperature deposition and annealing, the main phase of SmFe<sub>3</sub> or SmFe<sub>7</sub> formed at a composition ratio of SmFe<sub>1.9</sub> or SmFe<sub>1.6</sub>, and the main phase of SmFe<sub>2</sub> formed only when the Fe content decreased to SmFe or SmFe<sub>0.5</sub>; by depositing a 50 nm Ta layer, the film mainly consisted of Sm<sub>2</sub>Fe<sub>17</sub> phase and α-Fe at the SmFe<sub>9</sub> composition ratio, and when the Fe content was lowered to SmFe<sub>3</sub>, it mainly consisted of Sm<sub>2</sub>Fe<sub>17</sub> and SmFe<sub>3</sub> phases; further reducing the Fe content to near the stoichiometric ratio of SmFe<sub>2</sub> ( $x = 1.9$ ), the main phase of SmFe<sub>2</sub> formed in the Sm-Fe film. With the deposition of the Ta capping layer before annealing, pure SmFe<sub>2</sub> phase films (SmFe<sub>1.9</sub>(500 °C)/Ta(BA)–(700 °C, 1 h)) are successfully obtained by depositing at 500 °C and annealing at 700 °C for 1 h. Compared to the main phase SmFe<sub>2</sub> films prepared without the Ta capping layer, the SmFe<sub>1.9</sub>(500 °C)/Ta(BA)–(700 °C, 1 h) films exhibit a higher magnetostriction coefficient due to the formation of a purer SmFe<sub>2</sub> phase. The magnetostrictive coefficient is –234 ppm, lower than values reported in some literature, possibly due to the thicker silicon substrate. Consequently, under a magnetic field perpendicular to the film surface, the SmFe<sub>1.9</sub>(500 °C)/Ta(BA)–(700 °C, 1 h) films demonstrate significantly superior magnetic properties in the direction perpendicular to the film surface compared to films with other compositions. This highly perpendicular anisotropic film demonstrates significantly higher coercivity in the perpendicular direction, reaching 2427 Oe, surpassing 650 Oe reported in the literature for films close to the composition of SmFe<sub>2</sub>. The deposition of the Ta capping layer effectively suppresses the volatilization of Sm and facilitates the fabrication of films with desired phases. The success of the fabrication of good perpendicularly anisotropic magnetic films with pure SmFe<sub>2</sub> phase holds significant research value for the application in functional materials and devices.

**Author Contributions:** Conceptualization, J.Z., F.W., S.L. and H.S.; methodology, J.Z.; experimentation, S.L.; analysis and validation, J.Z., S.L. and H.S.; data curation, S.L. and F.W.; writing—original draft preparation, S.L. and J.Z.; writing—review and editing, S.L., J.Z. and H.S.; supervision, J.Z. and H.S. All authors have read and agreed to the published version of the manuscript.

**Funding:** This work was supported by the National Key Research and Development Program of China No.2021YFB3500303 and 2023YFB3507001; National Natural Science Foundation of China No.51971234; NSAF Joint Fund of China No. U2130124.

**Institutional Review Board Statement:** Not applicable.

**Informed Consent Statement:** Not applicable.

**Data Availability Statement:** Data are contained within the article.

**Conflicts of Interest:** The authors declare no conflicts of interest.

## References

1. Hu, S.; Cazorla, C.; Xiang, F.; Ma, H.; Wang, J.; Wang, J.; Wang, X.; Ulrich, C.; Chen, L.; Seidel, J. Strain Control of Giant Magnetic Anisotropy in Metallic Perovskite SrCoO<sub>3-δ</sub> Thin Films. *ACS Appl. Mater. Interfaces* **2018**, *10*, 22348–22355. [[CrossRef](#)] [[PubMed](#)]
2. Lu, Z.; Wen, L.; Feng, J.; Zheng, X.; Lao, B.; Li, S.; Zhao, K.; Gong, L.; Yang, H.; Chen, G.; et al. Orientation-Driven Strong Perpendicular Magnetic Anisotropy in La<sub>0.67</sub>Sr<sub>0.33</sub>MnO<sub>3</sub>-SrIrO<sub>3</sub> Heterostructures. *ACS Appl. Electron. Mater.* **2023**, *5*, 5633–5641. [[CrossRef](#)]
3. Sharma, S.; Hildebrandt, E.; Major, M.; Komissinskiy, P.; Radulov, I.; Alff, L. CeCo<sub>5</sub> thin films with perpendicular anisotropy grown by molecular beam epitaxy. *J. Magn. Magn. Mater.* **2018**, *452*, 80–85. [[CrossRef](#)]
4. Wu, Y.; Yang, Q.; Zhang, D.; Zhang, Y.; Rao, Y.; Wen, Q.; Syvorotka, I.I.; Zhang, H. The submicron garnet film with perpendicular magnetic anisotropy prepared by liquid phase epitaxy method. *J. Magn. Magn. Mater.* **2020**, *506*, 166689. [[CrossRef](#)]
5. Huang, C.-F.; Sun, A.-C.; Chang, H.W.; Yuan, F.-T.; Chang, S.T.; Chang, W.C. Improved perpendicular magnetic anisotropy of Pr-Fe-B films with Ta underlayer. *J. Alloys Compd.* **2014**, *584*, 185–189. [[CrossRef](#)]
6. Zhu, S.; Fu, J.; Li, H.; Zhu, L.; Hu, Y.; Xia, W.; Zhang, X.; Peng, Y.; Zhang, J. Direct Observation of Magnetocrystalline Anisotropy Tuning Magnetization Configurations in Uniaxial Magnetic Nanomaterials. *ACS Nano* **2018**, *12*, 3442–3448. [[CrossRef](#)] [[PubMed](#)]
7. Tudu, B.; Tiwari, A. Recent Developments in Perpendicular Magnetic Anisotropy Thin Films for Data Storage Applications. *Vacuum* **2017**, *146*, 329–341. [[CrossRef](#)]
8. Wu, G.; Wang, D.; Verma, N.; Rao, R.; Cheng, Y.; Guo, S.; Cao, G.; Watanabe, K.; Taniguchi, T.; Lau, C.N.; et al. Enhancing Perpendicular Magnetic Anisotropy in Garnet Ferrimagnet by Interfacing with Few-Layer WTe<sub>2</sub>. *Nano Lett.* **2022**, *22*, 1115–1121. [[CrossRef](#)] [[PubMed](#)]
9. Takei, S.; Liu, X.; Morisako, A. The property of multilayered SmCo<sub>5</sub> film with perpendicular magnetic anisotropy. *Phys. Status Solidi A* **2007**, *204*, 4166–4169. [[CrossRef](#)]
10. Sharma, S.; Hildebrandt, E.; Sharath, S.U.; Radulov, I.; Alff, L. YCo<sub>5±x</sub> thin films with perpendicular anisotropy grown by molecular beam epitaxy. *J. Magn. Magn. Mater.* **2017**, *432*, 382–386. [[CrossRef](#)]
11. Ma, T.; Jiao, J.; Li, Z.; Qiao, L.; Wang, T.; Li, F. Micrometer thick soft magnetic films with magnetic moments restricted strictly in plane by negative magnetocrystalline anisotropy. *J. Magn. Magn. Mater.* **2017**, *444*, 119–124. [[CrossRef](#)]
12. Hirose, T.; Komori, T.; Gushi, T.; Toko, K.; Suemasu, T. Perpendicular magnetic anisotropy in ferrimagnetic Mn<sub>4</sub>N films grown on (LaAlO<sub>3</sub>)<sub>0.3</sub>(Sr<sub>2</sub>TaAlO<sub>6</sub>)<sub>0.7</sub>(0 0 1) substrates by molecular beam epitaxy. *J. Cryst. Growth* **2020**, *535*, 125566. [[CrossRef](#)]
13. Li, H.; Wei, L.; Hong, Y.; Zhang, Y.; Qiu, Z.; Wang, G.; Zhao, L.; Liu, X.; Zhang, X.; Chen, D.; et al. Microstructure and Magnetic Anisotropy of SmCo-Based Films Prepared via External Magnetic Field Assisted Magnetron Sputtering. *Adv. Eng. Mater.* **2022**, *25*, 2101456. [[CrossRef](#)]
14. Onoda, H.; Sukegawa, H.; Inoue, J.I.; Yanagihara, H. Strain Engineering of Magnetic Anisotropy in Epitaxial Films of Cobalt Ferrite. *Adv. Mater. Interfaces* **2021**, *8*, 2101034. [[CrossRef](#)]
15. Romero, J.J.; Sastre, R.; Palomares, F.J.; Pigazo, F.; Cuadrado, R.; Cebollada, F.; Hernando, A.; González, J.M. Polymer Bonded Anisotropic Thick Hard Films for Micromotors/Microgenerators. *J. Iron Steel Res. Int.* **2006**, *13*, 240–251. [[CrossRef](#)]
16. Lee, H.S.; Cho, C.D.; Lee, U. Effect of Film Thicknesses of TbFe and SmFe on Magnetostrictions for Micro-Wireless Actuators. *Key Eng. Mater.* **2006**, *326–328*, 285–288. [[CrossRef](#)]
17. Kumar, K. RETM5 and RE2TM17 permanent magnets development. *J. Appl. Phys.* **1988**, *63*, R13–R57. [[CrossRef](#)]
18. Gjoka, M.; Sarafidis, C.; Giaremis, S. Towards Production of Cost-Effective Modification of SmCo<sub>5</sub>-Type Alloys Suitable for Permanent Magnets. *Materials* **2024**, *17*, 808. [[CrossRef](#)] [[PubMed](#)]
19. Yue, M.; Li, C.; Wu, Q.; Ma, Z.; Xu, H.; Palaka, S. A facile synthesis of anisotropic SmCo<sub>5</sub> nanochips with high magnetic performance. *Chem. Eng. J.* **2018**, *343*, 1–7. [[CrossRef](#)]
20. Kumari, K.; Kumar, A.; Park, S.-J.; Sharma, M.K.; Yadav, N.; Kumar, M.; Kumar, S.; Huh, S.-H.; Kim, J.-W.; Koo, B.-H. Effect of hydrazine on structural, morphological and magnetic properties of SmCo-Co nanocomposites. *Curr. Appl. Phys.* **2023**, *53*, 56–64. [[CrossRef](#)]
21. Konishi, T.; Nagai, H.; Nakata, Y.; Okutani, T. Microstructure and magnetic properties of Sm<sub>2</sub>Fe<sub>17</sub> alloy prepared by unidirectional solidification in microgravity. *J. Magn. Magn. Mater.* **2004**, *269*, 48–53. [[CrossRef](#)]
22. Peng, L.; Yang, Q.H.; Zhang, H.W.; Song, Y.Q.; Shen, J. Crystal structure and magnetic properties of hard magnetic Sm<sub>2</sub>Fe<sub>17</sub>N<sub>δ</sub> thin films with Co substitution. *J. Magn. Magn. Mater.* **2009**, *321*, 442–445. [[CrossRef](#)]
23. Christodoulou, C.N.; Takeshita, T. Hydrogenation and nitrogenation of SmFe<sub>3</sub>. *J. Alloys Compd.* **1993**, *191*, 279–285. [[CrossRef](#)]

24. Saito, T.; Horita, T.; Nishio-Hamane, D. Production of (Sm,Zr)Fe<sub>3</sub> magnets and their magnetic properties. *Mater. Sci. Eng. B* **2021**, *264*, 114990. [[CrossRef](#)]
25. Samata, H.; Fujiwara, N.; Nagata, Y.; Uchida, T.; Der Lan, M. Crystal growth and magnetic properties of SmFe<sub>2</sub>. *JPN J. Appl. Phys.* **1998**, *37*, 5544–5548. [[CrossRef](#)]
26. Zhou, B.-y.; Lei, D.-h.; Chen, S.-h.; Luo, H.-b. Magnetic properties and static–dynamic magnetostrictive characteristics for SmFe<sub>2</sub>/Fe exchange-coupled multilayers. *J. Magn. Magn. Mater.* **2011**, *323*, 2243–2247. [[CrossRef](#)]
27. Wang, L.; Du, Z.; Zhao, D. Influence of Magnetic Annealing on Properties of SmFe Thin Films. *J. Rare Earths* **2007**, *25*, 444–448. [[CrossRef](#)]
28. Hwang, S.W.; Kim, J.; Lim, S.U.; Kim, C.K.; Yoon, C.S. Magnetostrictive properties and microstructure of thermally annealed Sm–Fe thin films. *Mater. Sci. Eng. A* **2007**, *449–451*, 378–381. [[CrossRef](#)]
29. Honda, T.; Arai, K.I.; Yamaguchi, M. Fabrication of Magnetostrictive Actuators Using Rare-Earth (Tb,Sm)-Fe Thin-Films (Invited). *J. Appl. Phys.* **1994**, *76*, 6994–6999. [[CrossRef](#)]
30. Honda, T.; Hayashi, Y.; Yamaguchi, M.; Arai, K.I. Fabrication of Thin-Film Actuators Using Magnetostriction. *IEEE Transl. J. Magn. Jpn.* **1994**, *9*, 27–32. [[CrossRef](#)]
31. Quandt, E.; Seemann, K. Fabrication of giant magnetostrictive thin film actuators. In Proceedings of the Micro Electro Mechanical Systems—IEEE Proceedings, Amsterdam, The Netherlands, 29 January–2 February 1995; pp. 273–277. [[CrossRef](#)]
32. Li, G.; Li, M.; Wang, J.; Du, J.; Wang, K.; Wang, Q. Effect of high magnetic field on structure and magnetic properties of evaporated crystalline and amorphous Fe-Sm thin films. *J. Magn. Magn. Mater.* **2017**, *423*, 353–358. [[CrossRef](#)]
33. Choi, Y.S.; Lee, S.R.; Han, S.H.; Kim, H.J.; Lim, S.H. Magnetic properties of amorphous Sm-Fe and Sm-Fe-B thin films fabricated by radio-frequency magnetron sputtering. *J. Appl. Phys.* **1998**, *83*, 7270–7272. [[CrossRef](#)]
34. Shima, T.; Yokoyama, H.; Fujimori, H. Magnetostriction and magnetic properties of Sm-Fe-B and Tb-Fe-B thin films and multilayers. *J. Alloys Compd.* **1997**, *258*, 149–154. [[CrossRef](#)]
35. Honda, T.; Hayashi, Y.; Yamaguchi, M.; Arai, K.I. Magnetostriction of Sm-Fe Thin Films Fabricated by a Sputtering Method. *IEEE Transl. J. Magn. Jpn.* **1994**, *9*, 129–133. [[CrossRef](#)]
36. Honda, T.; Hayashi, Y.; Arai, K.I.; Ishiyama, K.; Yamaguchi, M. Magnetostriction of Sputtered Sm-Fe Thin-Films. *IEEE Trans. Magn.* **1993**, *29*, 3126–3131. [[CrossRef](#)]
37. Nishi, Y.; Matsumura, Y.; Kadowaki, A.; Masuda, S. Composition dependence on Compressive magnetostriction of Fe-Sm binary alloy thin films. *Mater. Trans.* **2005**, *46*, 3063–3066. [[CrossRef](#)]
38. Masuda, S.; Matsumura, Y.; Nishi, Y. Metallographic research of GM Sm-Fe alloy film. *J. Adv. Sci.* **2006**, *18*, 62–64. [[CrossRef](#)]
39. Lim, S.H.; Choi, Y.S.; Han, S.H.; Kim, H.J.; Shima, T.; Fujimori, H. Magnetostriction of Sm-Fe and Sm-Fe-B thin films fabricated by RF magnetron sputtering. *J. Magn. Magn. Mater.* **1998**, *189*, 1–7. [[CrossRef](#)]

**Disclaimer/Publisher’s Note:** The statements, opinions and data contained in all publications are solely those of the individual author(s) and contributor(s) and not of MDPI and/or the editor(s). MDPI and/or the editor(s) disclaim responsibility for any injury to people or property resulting from any ideas, methods, instructions or products referred to in the content.